Supplemental material

Juanes et al., https://doi.org/10.1083/jcb.201904165

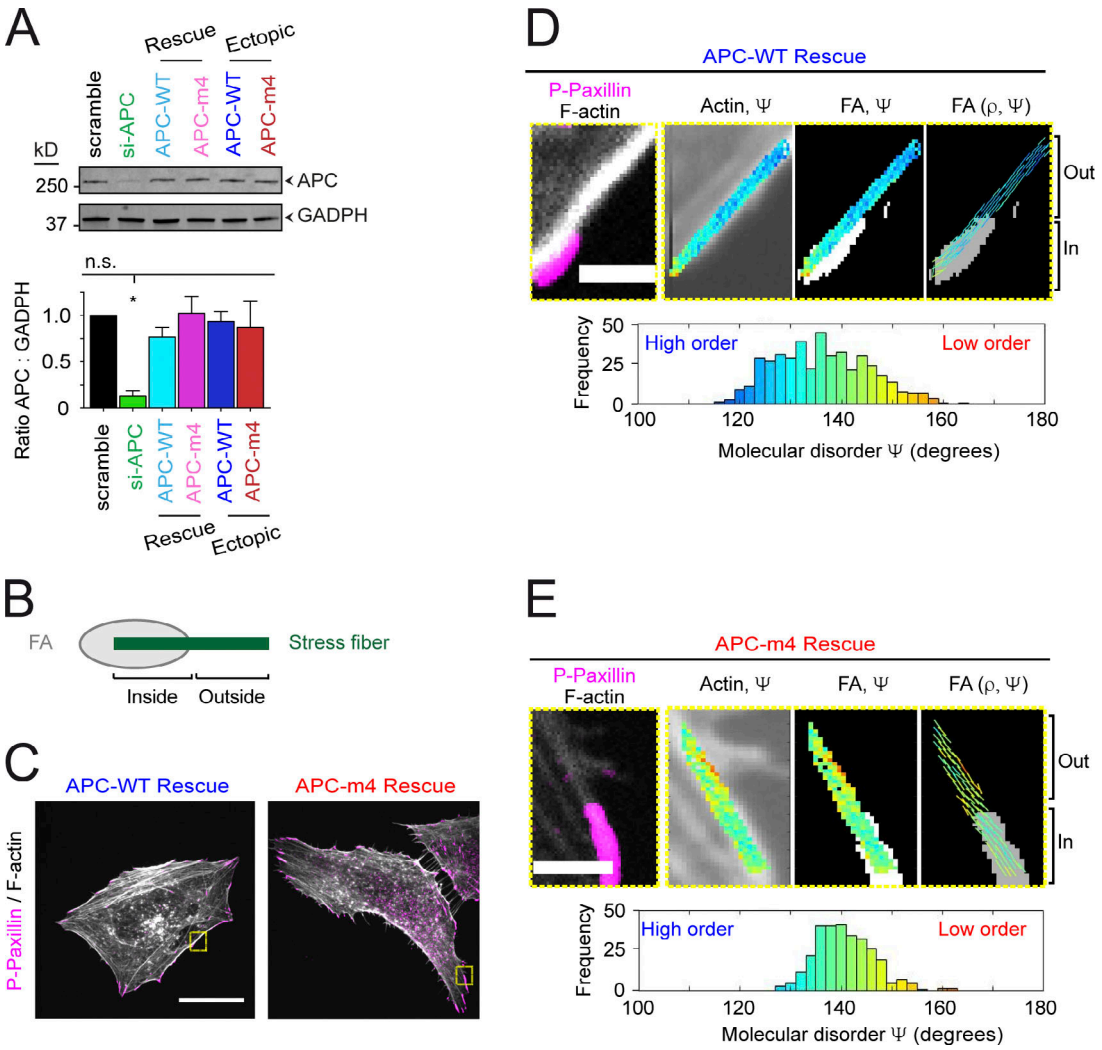

Figure S1. **APC-m4 disrupts the molecular order of F-actin at FAs.** Related to Fig. 1. All data are from U2OS cells, not micropatterned as in Fig. 2, C–I. **(A)** Western blot of whole cell extracts from U2OS cells treated with scramble RNAi (control), depleted of endogenous APC (si-APC), depleted of endogenous APC and rescued with refractory APC-WT or APC-m4 (rescue), and cells expressing the APC constructs without depleting endogenous APC (ectopic). Blots were probed with antibodies to APC and GAPDH (loading control). Graph (right) quantifies ratio of APC to GAPDH signals from blots. Data averaged from two independent experiments. Error bars, SEM. Statistical significance calculated by one-way ANOVA Holm–Sidak multiple comparisons test: (compared with scramble, and in order from left to right): *, $P < 0.05$; n.s., not significant. **(B)** Schematic of FA (gray) and stress fiber (green), highlighting ROIs analyzed for F-actin molecular organization by polarization-resolved microscopy. ROIs overlapping with FAs designated as "Inside"; ROIs just outside of FAs on the stress fiber designated "Outside." **(C)** Representative confocal images of cells depleted of endogenous APC and rescued with APC-WT or APC-m4. Cells were fixed and stained with Alexa Fluor 488–phalloidin (F-actin, gray) and phospho-paxillin antibodies (pink). Yellow boxes highlight areas analyzed in D and E. Scale bar, 20 µm. **(D)** Representative zooms from boxed region of APC-WT cell in C. Left panel shows overlay of Alexa Fluor 488–phalloidin (gray) and phospho-paxillin (pink). Remaining panels (left to right) show the color-coded molecular order (Ψ) super-imposed on Alexa Fluor 488–phalloidin (F-actin, gray); intensity-thresholded image of FA (white) superimposed with stick representation of Ψ (encoded in stick color); and mean orientation (ρ) encoded in stick orientation with thresholded image of FAs (gray). Histograms display Ψ value distribution (in degrees) from inside and outside ROIs combined ($<\Psi> = 136°$). Scale bar, 2 µm. **(E)** Same as D except APC-m4 cells ($<\Psi> = 145°$).

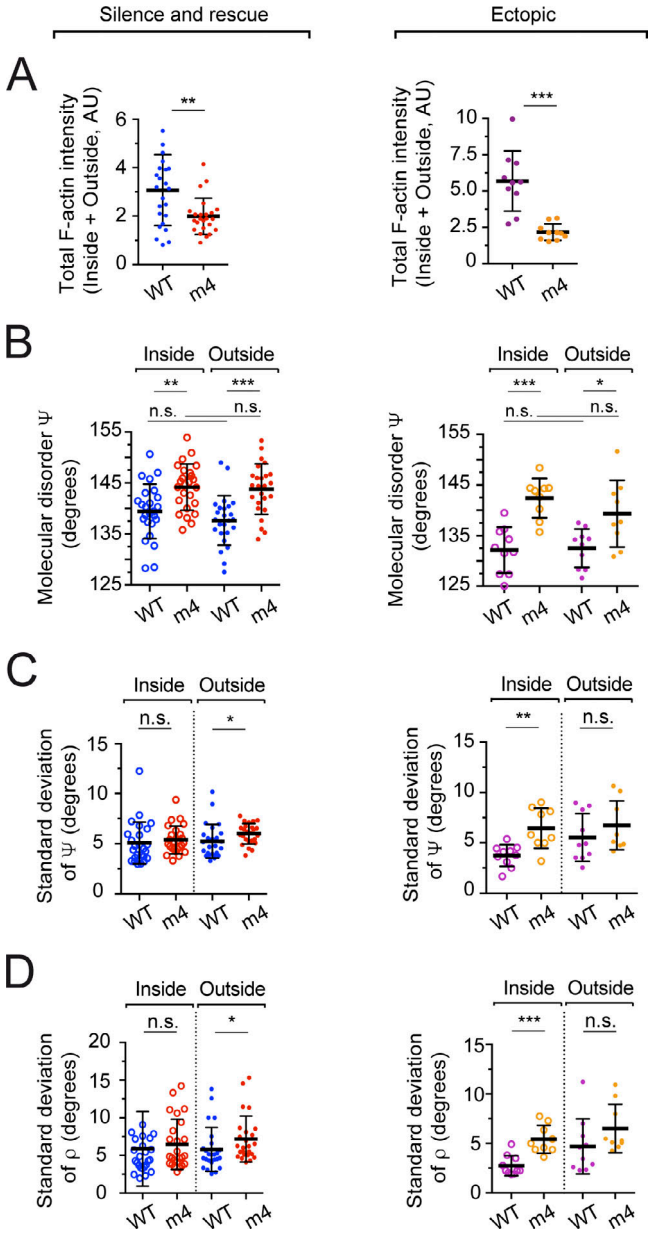

Figure S2. **APC-m4 disrupts the molecular order of F-actin at FAs.** Related to Fig. 1. All data are from U2OS cells grown on collagen dishes, but not micropatterned as in Fig. 2, C–I. Left panels are data from cells depleted of endogenous APC (si-APC) and expressing APC-WT or APC-m4 rescue plasmids (silence and rescue). Right panels are data from cells ectopically expressing APC-WT or APC-m4 (ectopic). **(A)** Total F-actin intensity from inside and outside ROIs combined. **(B)** Bee swarm plot showing average molecular order (Ψ) separately for inside and outside ROIs. **(C)** Bee swarm plot showing SD_Ψ separately for inside and outside ROIs. **(D)** Bee swarm plot showing SD_ρ separately for inside and outside ROIs. Data in left panels averaged from three independent experiments. n = 25 ROIs from $n \geq 15$ cells per condition. Error bars, SD. Statistical significance calculated by nonparametric Mann–Whitney two-tailed Student's t test: ***, P < 0.001; **, P < 0.01; *, P < 0.05; n.s., not significant. Data in right panels averaged from two independent experiments. n = 10 ROIs from n = 8 cells per condition. Error bars, SD. Statistical significance calculated by nonparametric Mann–Whitney two-tailed Student's t test: ***, P < 0.001; **, P < 0.01; *, P < 0.05; n.s., not significant.

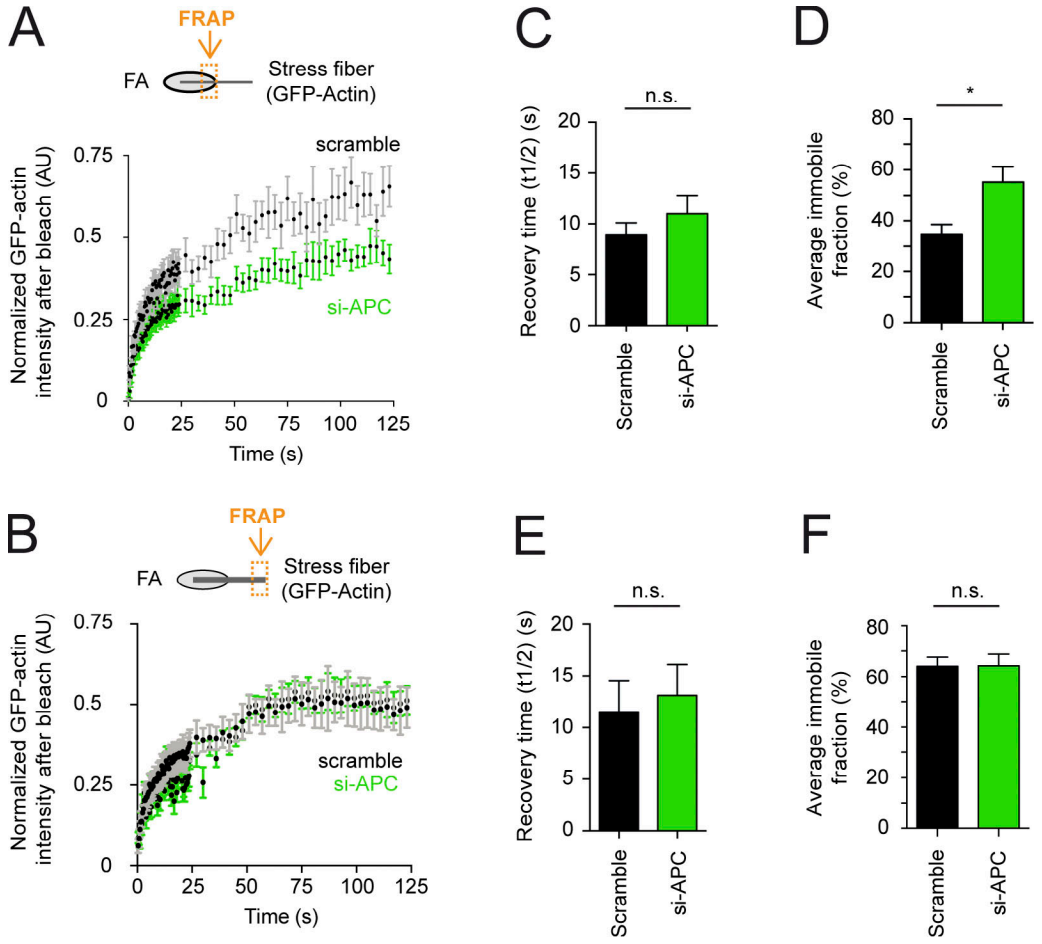

Figure S3. **Effects of APC depletion on actin dynamics in FAs and stress fibers.** Related to Fig. 2. All data are from U2OS cells treated with scramble RNAi (control) or depleted of endogenous APC (si-APC). **(A)** FRAP analysis, in which ROIs were selected where GFP-actin and mCherry-zyxin signals overlap (see orange box in cartoon). ROIs were then bleached and monitored for GFP-actin fluorescence recovery. Graphs show mean recovery profiles normalized to zero after bleaching. Data averaged from three independent experiments (n = 30 ROIs from n = 15 cells per condition). **(B)** FRAP experiments as in A except that ROIs were selected along stress fibers at a distance (> 5 µm) away from FAs (see orange box in cartoon). Graphs show mean recovery profiles normalized to zero after bleaching. Data averaged from three independent experiments (n = 30 ROIs from n = 15 cells per condition). **(C)** Average time to 50% maximal recovery for experiments in A. Error bars, SEM. Statistical significance calculated by nonparametric Mann–Whitney two-tailed Student's t test: n.s., not significant. **(D)** Average immobile fraction (does not recover in observation window) for experiments in A. Error bars, SEM. Statistical significance calculated by nonparametric Mann–Whitney two-tailed Student's t test: *, $P < 0.05$. **(E)** Average time to 50% maximal recovery for experiments in B. Error bars, SEM. Statistical significance calculated by nonparametric Mann–Whitney two-tailed Student's t test: n.s., not significant. **(F)** Average immobile fraction for experiments in B. Error bars, SEM. Statistical significance calculated by nonparametric Mann–Whitney two-tailed Student's t test: n.s., not significant.

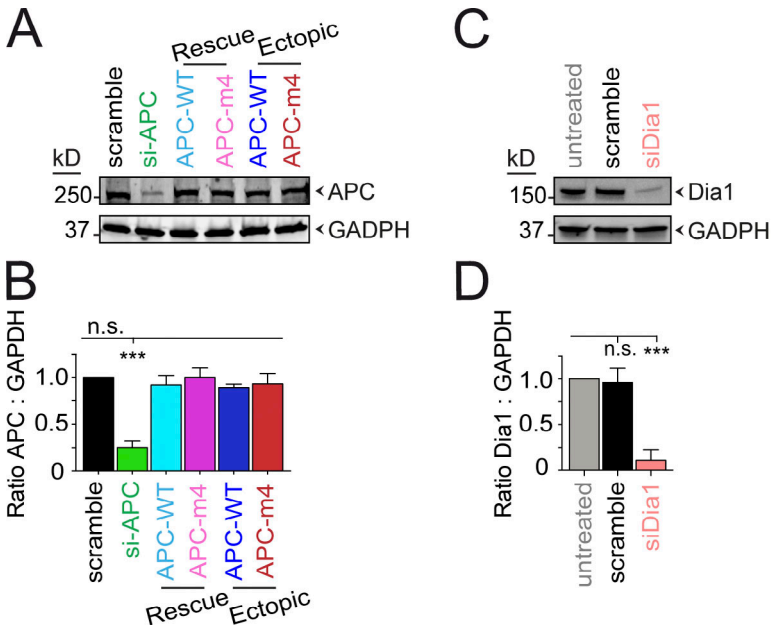

Figure S4. **Levels of APC and Dia1 in MDA-MB-231 cells.** Related to Fig. 4. **(A)** Western blot analysis of whole cell extracts from MDA-MB-231 cells treated with scramble RNAi (control), depleted of endogenous APC (si-APC), depleted of endogenous APC and rescued with refractory APC-WT or APC-m4 (rescue), and cells expressing the same APC constructs without depleting endogenous APC (ectopic). Blots were probed with antibodies to APC and GAPDH (loading control). **(B)** Quantification of the ratio of APC to GAPDH from blots as in A. Data averaged from two experiments. Error bars, SEM. Statistical significance calculated by ordinary one-way ANOVA Holm–Sidak multiple comparisons test (compared with scramble, and in order from left to right): ***, $P < 0.001$; n.s., not significant. **(C)** Western blot analysis of whole cell extracts from MDA-MB-231 cells that were untreated, control RNAi-treated (scramble), or Dia1-silenced (si-Dia1). Blots were probed with antibodies to Dia1 and GAPDH (loading control). **(D)** Quantification of the ratio of Dia1 to GAPDH from blots as in C. Data averaged from four separate experiments. Error bars, SEM. Statistical significance calculated by ordinary one-way ANOVA Holm–Sidak multiple comparisons test (compared with scramble, and in order from left to right): ***, $P < 0.001$; n.s., not significant.

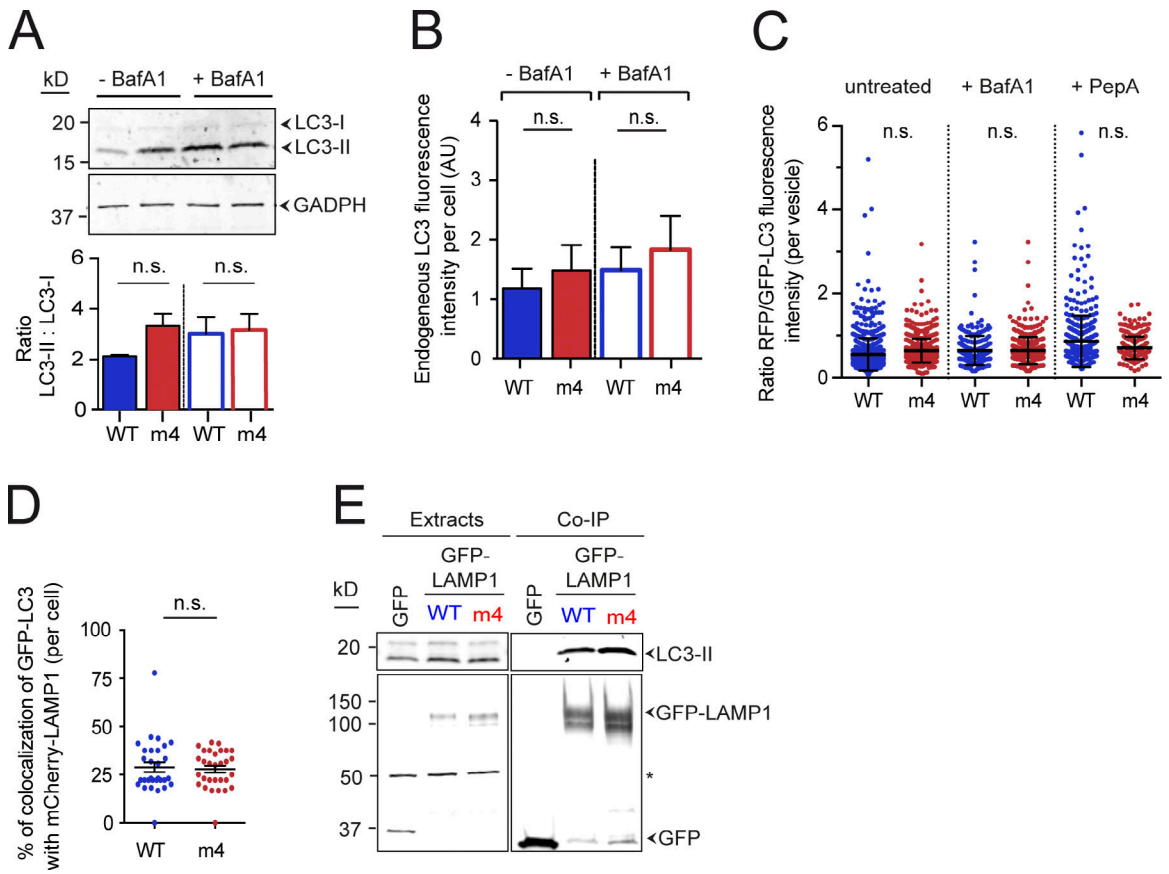

Figure S5. **APC-m4 expression does not alter global autophagy.** Related to Fig. 6. All data are from MDA-MB-231 cells expressing APC constructs (APC-WT or APC-m4), using fixed or live imaging as indicated. **(A)** APC-m4 expression does not change total cellular levels of LC3-I and LC3-II. Western blotting of whole cell extracts from untreated cells or cells treated for 2 h with 100 nM Bafilomycin 1 (BafA1; an autophagy inhibitor). Blots were probed with antibodies to LC3, which detects both lipidated–LC3-II and nonlipidated–LC3-I, as indicated by arrows, and GAPDH (loading control). The graph below quantifies ratio of LC3-II to LC3-I. Data averaged from two independent experiments. Error bars, SEM. Statistical significance calculated by nonparametric Mann–Whitney two-tailed Student's *t* test: n.s., not significant. **(B)** APC-m4 expression does not change total cellular levels of LC3 detected by immunostaining. Fluorescence intensity of endogenous LC3, detected by antibody staining, from cell images treated as in A. Data averaged from three independent experiments ($n \geq 20$ cells per condition). Error bars, SEM. Statistical significance calculated by nonparametric Mann–Whitney two-tailed Student's *t* test: n.s., not significant. **(C)** APC-m4 expression does not change the maturation state of autophagosomes trafficking from ER to fuse with lysosomes. Cells were transduced with the pH-sensitive Premo autophagy tandem sensor (RFP-GFP-LC3B), and then treated with Bafilomycin 1 (autophagy inhibitor) or Pepstatin A (lysosome inhibitor) as indicated. Transitions from the autophagosome (yellow) to the autolysosome (red) were visualized by loss of GFP fluorescence (due to acidification following autophagosome-lysosomal fusion). Graphed is the ratio of RFP-LC3 to GFP-LC3 fluorescence in each LC3 vesicle, which provides an indication of autophagosome maturation state. Data averaged from three independent experiments (n = 280–958 vesicles from n = 10–50 cells per condition). Error bars, SEM. Statistical significance calculated by one-way ANOVA Holm–Sidak multiple comparisons test: n.s., not significant. **(D)** APC-m4 expression does not change the percentage of autophagosomes in cells undergoing fusion with lysosomes. Live imaging was used to determine the percent colocalization of GFP-LC3 (autophagosomes) with mCherry-LAMP1 (lysosome/late endosome marker) to assess autophagosome-lysosome fusion. Data averaged from two independent experiments (n = 30 cells per condition). Error bars, SEM. Statistical significance calculated by nonparametric Mann–Whitney two-tailed Student's *t* test: n.s., not significant. **(E)** APC-m4 expression does not alter coimmunoprecipitation of endogenous LC3 with GFP-LAMP1. GFP-LAMP1 was pulled down out of cell lysates using GFP–Trap-A agarose beads. Cells transfected with empty vector (expressing GFP alone instead of GFP-LAMP1) were used as a negative control. A nonspecific band that cross-reacts with the antibody is shown as with an asterisk.

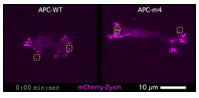

Video 1. **FA dynamics in migrating cells.** Related to Fig. 4. Representative examples of time-lapse TIRF imaging of FAs (mCherry-zyxin, pink) in migrating MDA-MB-231 cells ectopically expressing APC-WT or APC-m4, as indicated. Yellow boxes that appear during the video highlight the same four FAs shown as examples in Fig. 4, A and B. Images were acquired every 10 s. Video is shown at seven frames per second. Scale bar, 10 µm. .

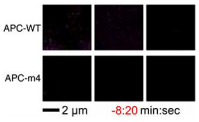

Video 2. **Lifetimes of individual FAs.** Related to Fig. 4. Representative examples of time-lapse TIRF imaging of mCherry-zyxin (FA marker) assembly and disassembly in migrating MDA-MB-231 cells ectopically expressing APC-WT or APC-m4, as indicated. The arrows that appear during the video indicate the point of FA peak growth or maturation (maximum intensity), which was set to time = 0. Negative numbers correspond to the FA assembly phase, and positive numbers to disassembly phase. Images were acquired every 10 s. Video is shown at seven frames per second. Scale bar, 2 µm.

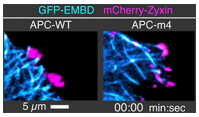

Video 3. **Microtubule dynamics at FAs in migrating cells.** Related to Fig. 5. Representative examples of time-lapse TIRF imaging of microtubules (3xGFP-EMDB, cyan) and FAs (mCherry-zyxin, pink) in migrating MDA-MB-231 cells ectopically expressing full-length APC-WT or APC-m4, as indicated. Images were acquired every 5 s. Video is shown at seven frames per second. Scale bar, 5 µm.

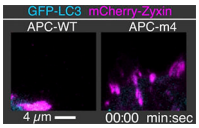

Video 4. **Autophagosome dynamics at FAs in migrating cells.** Related to Fig. 6. Representative examples of time-lapse TIRF imaging of autophagosomes (GFP-LC3, cyan) and FAs (mCherry-zyxin, pink) in migrating MDA-MB-231 cells ectopically expressing APC-WT or APC-m4, as indicated. The yellow arrows that appear during the video highlight a few examples of autophagosome interactions with FAs, starting from the time of first contact of the autophagosome with the FA to complete disassembly of the FA. Images were acquired every 10 s. Video is shown at seven frames per second. Scale bar, 4 µm.